Journal of The Electrochemical Society, **157** (3) A348-A354 (2010)
0013-4651/2010/157(3)/A348/7/$28.00 © The Electrochemical Society

Structural and Electrochemical Properties of $LiNi_{0.5}Mn_{0.5}O_2$ Thin-Film Electrodes Prepared by Pulsed Laser Deposition

H. Xia,[a] Y. S. Meng,[b,*,c] M. O. Lai,[a] and L. Lu[a,z]

[a]*Department of Mechanical Engineering, National University of Singapore, Singapore 117576*
[b]*Department of Material Science and Engineering, University of Florida, Gainesville, Florida 32611-6400, USA*

$LiNi_{0.5}Mn_{0.5}O_2$ thin-film electrodes have been prepared by pulsed laser deposition followed by postannealing at different temperatures. The microstructural and morphological characterizations using X-ray diffraction, field-emission-scanning electron microscopy, and Raman spectroscopy measurements show that the structure and phase purity of the thin films are highly dependent on the postannealing temperatures. The films that are postannealed at low temperatures exhibit a relatively lower degree of crystallinity, but a high phase purity. The electronic structure and cation disorder of the $LiNi_{0.5}Mn_{0.5}O_2$ thin-film samples are further investigated by X-ray photoelectron spectroscopy and magnetic property measurement. The charge/discharge behaviors of the thin films that are postannealed at different temperatures indicate that phase-pure $LiNi_{0.5}Mn_{0.5}O_2$ thin films can only be prepared at low annealing temperatures. Electrochemical impedance spectroscopy studies on thin-film electrodes indicate a strong dependence of charge-transfer resistance on the electrode potential. The rate capability and cycling stability in different voltage windows of $LiNi_{0.5}Mn_{0.5}O_2$ thin-film electrodes are further investigated. The relationship between the microstructure and electrochemical properties of $LiNi_{0.5}Mn_{0.5}O_2$ thin-film electrodes has been discussed.
 [DOI: 10.1149/1.3294719]

Manuscript received October 29, 2009. Published February 4, 2010.

All-solid-state thin-film Li-ion microbatteries have attracted attention due to their potential applications as power sources for micro- and nanodevices, such as microsensors, implantable medical devices, smart cards, and nano-electromechanical systems. To realize microbatteries for various applications, it is imperative to develop a high quality thin-film cathode with high energy density, high reversibility, stable voltage range, and low cost. Extensive research has been carried out to synthesize and characterize lithium transitional metal oxide thin films in view of their potential application as the cathode film for microbatteries.[1-3] Previous works on developing thin-film cathodes have been focused on $LiCoO_2$ thin-film electrodes because $LiCoO_2$ has been the most successful cathode materials for lithium-ion batteries. However, due to the structural instability of $LiCoO_2$ at low lithium concentration, only half of the theoretical capacity can be utilized ($\sim$140 mAh/g). In addition, the toxicity and high cost of Co limit its further application. Therefore, much effort has been devoted to searching for alternative cathode materials to replace $LiCoO_2$. Among the newly developed cathode materials, $LiNi_{0.5}Mn_{0.5}O_2$ is one of the most promising candidates due to its low cost, improved safety, and much larger reversible capacity compared to $LiCoO_2$.[4-6] Advanced properties of $LiNi_{0.5}Mn_{0.5}O_2$ make it promising to be utilized for microbatteries. As a cathode material, the study on thin-film electrodes without any binders or conductive additives provides more insights in the intrinsic properties of the material. However, very limited research has been done on the layered $LiNi_{0.5}Mn_{0.5}O_2$ thin-film electrodes until now.[7,8]

In our previous work, we have demonstrated that pulsed laser deposition (PLD) can be successfully utilized to prepare layered $LiNi_{0.5}Mn_{0.5}O_2$ thin-film electrodes.[9] The substrate plays an important role in growing layered $LiNi_{0.5}Mn_{0.5}O_2$ thin films. In addition to the substrate effect, the postannealing process after PLD is also critical to the microstructure and electrochemical properties of $LiNi_{0.5}Mn_{0.5}O_2$ thin films. In this work, $LiNi_{0.5}Mn_{0.5}O_2$ thin films are prepared at different postannealing temperatures. The effect of postannealing temperature on the microstructure and electrochemical properties of the $LiNi_{0.5}Mn_{0.5}O_2$ thin films is investigated. Phase-pure layered $LiNi_{0.5}Mn_{0.5}O_2$ thin-film electrodes are then used as the ideal samples to study electrochemical impedance spectroscopy (EIS) at different charge states, rate capability, cycling stability in different voltage windows, and long time cycling stability in liquid electrolyte.

Experimental

$LiNi_{0.5}Mn_{0.5}O_2$ thin films were deposited on the Au substrates by PLD. The target was prepared by sintering a mixture of LiOH, NiO, and MnO_2 (99%, Alfa Aesar) at 1000°C in air for 12 h. To compensate the Li loss during the sintering and deposition, excess LiOH was added leading to a Li/(Ni + Mn) ratio of 1.5 in the starting mixture. A Lambda Physik KrF excimer laser with a wavelength of 248 nm was used in the deposition. The laser fluence and repletion rate were controlled at 2 J/cm^2 and 10 Hz, respectively. The thin films were deposited at a substrate temperature of 550°C with an oxygen partial pressure of 2 Torr. The postannealing of the thin films was conducted in the furnace with an oxygen flow at a temperature from 750 to 950°C for 3 h.

The structure and the crystallinity of the films were investigated using a Shimadzu X-ray diffractometer (XRD)-6000 with Cu Kα radiation and a Jobin–Yvon T6400 micro-Raman system equipped with a charge-coupled device detector. The Raman spectra were recorded using the 514.5 nm line of an Ar^+ laser at a power level of 5 mW. The morphology of the thin films was investigated through field-emission-scanning electron microscopy (FESEM). X-ray photoelectron spectroscopy (XPS) analysis was performed on the thin film with a VG ESCALAB MK spectrometer using Al Kα radiation (1486.6 eV). An analyzer with a pass energy of 20 eV was adopted, and a C 1s peak at 284.6 eV due to adventitious carbon was used as an internal reference. A superconducting quantum interference device magnetometer was used to measure the dependence of the magnetization upon the applied field at 10 K for both the thin-film and powder samples.

The electrochemical properties of the as-prepared thin-film electrodes were investigated by a Solartron 1287 electrochemical interface combined with a Solartron 1260 frequency response analyzer. The laboratory-made Swagelok-type cells consist of a Li metal foil counter electrode, a $LiNi_{0.5}Mn_{0.5}O_2$ thin-film working electrode, and 1 M $LiPF_6$ in ethylene carbonate/diethyl carbonate (1/1, vol %) as the electrolyte. The loading of the thin-film electrode obtained by microbalance is usually around 0.20 mg with an error of about $\pm$0.01 mg. The galvanostatic charge/discharge measurements were carried out in different voltage ranges at different current densities.

* Electrochemical Society Active Member.
[c] Present address: Department of Nano Engineering, University of California San Diego, La Jolla, California 92093-0448, USA.
[z] E-mail: mpeluli@nus.edu.sg

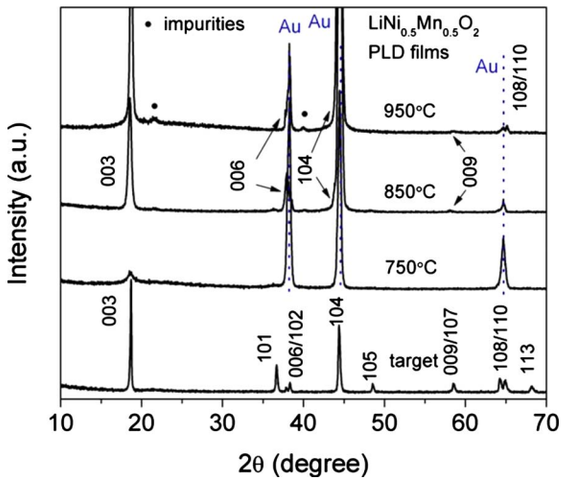

Figure 1. (Color online) XRD spectra of the $LiNi_{0.5}Mn_{0.5}O_2$ thin films annealed at different temperatures and of the target.

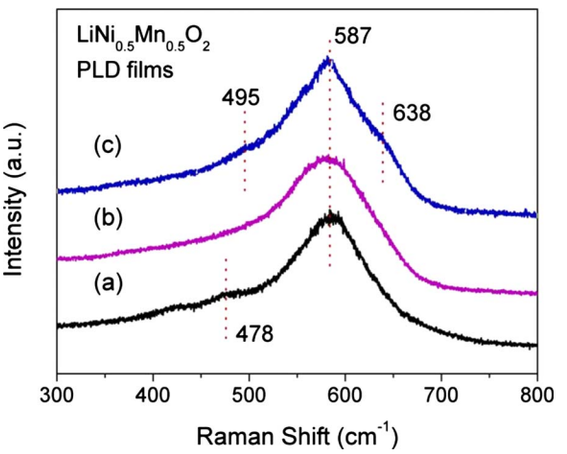

Figure 2. (Color online) Raman spectra of the $LiNi_{0.5}Mn_{0.5}O_2$ thin films annealed at different temperatures: (a) 750, (b) 850, and (c) 950°C.

The EIS measurements were conducted at various electrode potentials in the frequency range from 100 kHz to 3 mHz. The EIS data were analyzed by equivalent circuit fitting using the ZView2 software of Scribner Co.

Results and Discussion

The XRD spectra of the $LiNi_{0.5}Mn_{0.5}O_2$ thin films postannealed at different temperatures and of the target are shown in Fig. 1. The XRD spectrum of the target can be indexed based on the α-$NaFeO_2$ structure with space group $R\bar{3}m$. The existence of doublets at (006)/(102) and (108)/(110) clearly indicates the layered structure of the target.[10] At a low annealing temperature of 750°C, only one small (003) peak from the film can be observed from the XRD spectrum. As the annealing temperature increases, the (003) peak increases significantly, indicating the improvement of crystallization. At high annealing temperatures, other reflection peaks such as (101), (104), and (110) are very weak, indicating a preferred (003) texture of the film. Although no impurity peaks can be detected from the XRD spectra for the 750 and 850°C annealed thin films, two impurity peaks can be observed from the XRD spectrum for the 950°C annealed thin film. The two impurity peaks are attributed to Li_2MnO_3 and Mn_2O_3 probably due to the severe Li loss at such a high annealing temperature.

To further investigate the structure of the films, Raman scattering (RS) measurements were carried out on the thin-film samples annealed at different temperatures. Figure 2 shows the RS spectra of the $LiNi_{0.5}Mn_{0.5}O_2$ thin films annealed at 750, 850, and 950°C, respectively. The material with the layered structure normally displays two Raman-active modes, A_{1g} and E_g, as predicted by the theoretical factor group analysis of the $R3m$ rock salt structure.[11] As shown in Fig. 2a, the 750°C annealed thin films exhibits two Raman bands peaked at 478 and 587 cm^{-1}. The Raman bands at 478 and 587 cm^{-1} match well with Raman-active A_{1g} and E_g modes reported for the layered $LiNi_{0.5}Mn_{0.5}O_2$,[12] $LiNi_{0.8}Co_{0.2}O_2$,[13] and $LiNi_{1/3}Co_{1/3}Mn_{1/3}O_2$ [14] powders. For the 850°C annealed thin film, the RS spectrum is similar to that of the 750°C annealed samples. As the anneal temperature is further increased to 950°C, two shoulders at 495 and 638 cm^{-1} could be observed in addition to the strong peak at 587 cm^{-1}. The Raman bands peaked at 495 and 638 cm^{-1} are a characteristic of the cubic spinel phase such as $LiMn_2O_4$ and $LiNi_{0.5}Mn_{1.5}O_4$.[15] It is speculated that the Li loss at such a high annealing temperature is quite severe, leading to the formation of some spinel phases in the film. It has been reported that Li loss could be the reason that causes the formation of impurity phases during high vacuum or high temperature processes for the preparation of the layered structure thin films.[16] Both the XRD and Raman results indicate that phase-pure layered $LiNi_{0.5}Mn_{0.5}O_2$ thin films cannot be prepared at a high annealing temperature of 950°C.

The surface morphologies of $LiNi_{0.5}Mn_{0.5}O_2$ thin films annealed at different temperatures are shown in Fig. 3. As shown in Fig. 3a, the film annealed at 750°C is composed of spherical grains with an average grain size of about 100–200 nm. The spherical grains that developed on the Au substrate are similar to those observed in the layered $LiCoO_2$ and $LiNi_{0.8}Co_{0.2}O_2$ thin films grown by PLD.[14,17] The grains are not very closely packed with many holes embedded in the film, resulting in a porous structure. This porous morphology is probably attributed to the rough surface of the Au substrate as a very dense film could be prepared when using a polished Au substrate with a smooth surface (results not shown here). As the annealing temperature is increased to 850°C, a similar morphology of the film can be obtained but with better defined grain boundaries, indicating an improved crystallinity. As the annealing temperature is increased to 950°C, a significant morphology change could be observed with a pronouncedly increased grain size of microrange. As shown in Fig. 3c, some of the grains exhibit hexagonal shapes, which is characteristic of a well-crystallized layered structure. To evaluate the thickness of the film, the cross-sectional FESEM of a

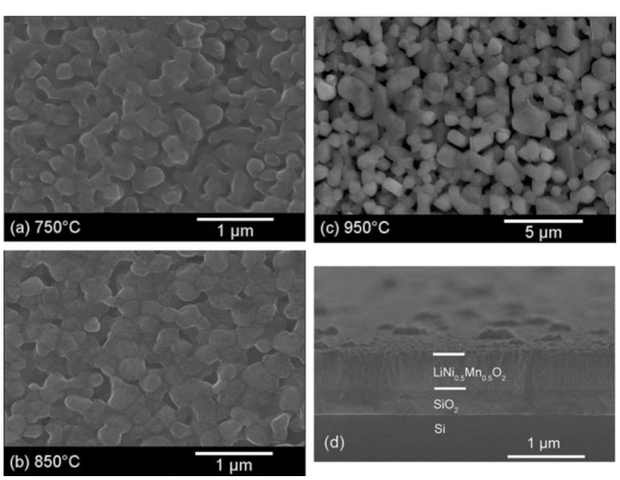

Figure 3. FESEM images of the $LiNi_{0.5}Mn_{0.5}O_2$ thin films annealed at different temperatures: (a) 750, (b) 850, and (c) 950°C and (d) cross-sectional FESEM image of the $LiNi_{0.5}Mn_{0.5}O_2$ thin film deposited on the SiO_2/Si substrate.

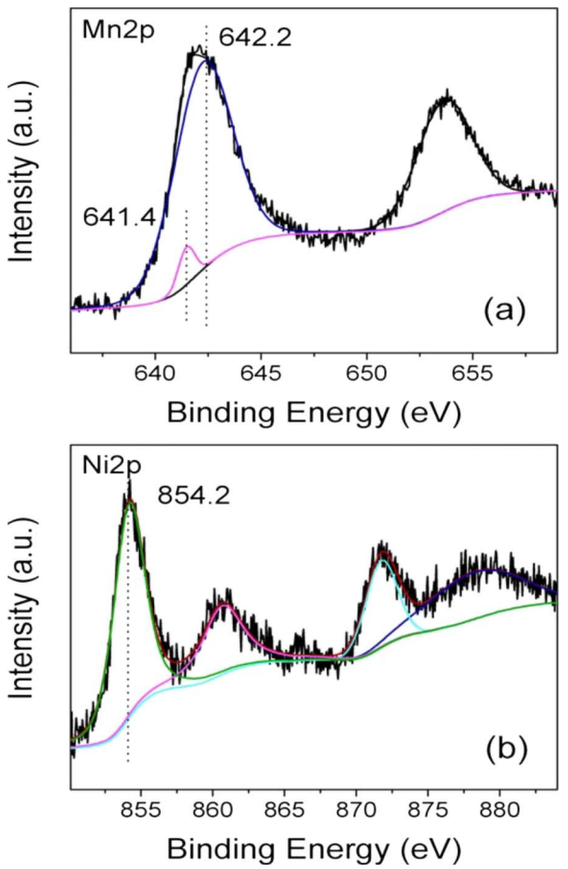

Figure 4. (Color online) XPS spectra of (a) Mn $2p_{3/2}$ and (b) Ni $2p_{3/2}$ of the $LiNi_{0.5}Mn_{0.5}O_2$ thin film annealed at 750°C.

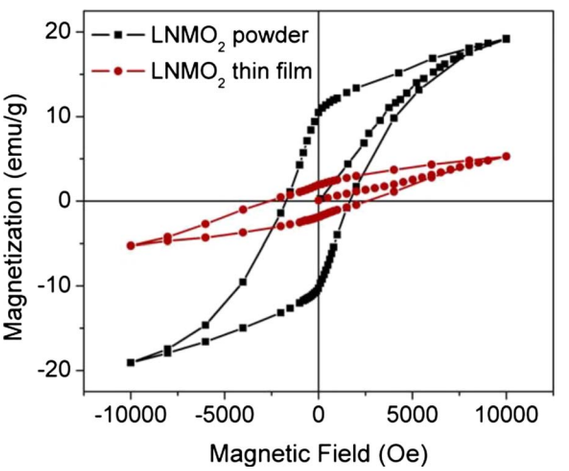

Figure 5. (Color online) Magnetization curves of the $LiNi_{0.5}Mn_{0.5}O_2$ powder (synthesized at 1000°C) and of the $LiNi_{0.5}Mn_{0.5}O_2$ thin film (750°C annealed sample).

$LiNi_{0.5}Mn_{0.5}O_2$ thin film deposited on a SiO_2/Si substrate is shown in Fig. 3d. It can be seen that the film is homogeneous and the average thickness is about 500 nm.

To investigate the oxidation states of Ni and Mn in the $LiNi_{0.5}Mn_{0.5}O_2$ thin films grown on the Au substrates, XPS was carried out on the thin-film samples annealed at 750°C. Figure 4a and b shows the narrow scan spectra of Mn 2p and Ni 2p, respectively. As shown in Fig. 4a, the Mn $2p_{3/2}$ XPS spectrum can be best fitted with two peaks with a major peak at 642.2 eV and a minor peak at 641.4 eV. The major peak corresponds to Mn^{4+}, while the minor peak corresponds to Mn^{3+}. As shown in Fig. 4b, the Ni $2p_{3/2}$ XPS spectrum can be best fitted with one peak with a binding energy of 854.2 eV, which indicates that almost all Ni in the film exist in a 2+ oxidation state. Therefore, most Mn and Ni in the film exist in 4+ and 2+, respectively, which agrees well with a previous report on composite $LiNi_{0.5}Mn_{0.5}O_2$ electrodes with a layered structure.[18]

For $LiNi_{0.5}Mn_{0.5}O_2$, the ideal layered structure with a perfect separation between Li and transition-metal cations into alternating layers could not be achieved. There is always an 8–12% exchange of occupancy of Li^+ and Ni^{2+} ions due to their similar ionic radius. A high degree of Li/Ni disorder leads to poor rate capability due to slow Li mobility in this less ordered structure.[4] To evaluate the Li/Ni disorder in the thin-film sample and to compare it with the powder sample, the magnetization curves of both the thin-film and powder samples have been measured. The Ni ions in the Li layers result in the formation of ferrimagnetic clusters, leading to an increase in the magnetic hysteresis observed at low temperatures.[19] The magnetization curves of a thin-film sample (750°C annealed sample) and powder sample are shown in Fig. 5. It can be seen that both thin-film and powder samples exhibit obvious magnetic hysteresis loops, indicating that a certain amount of Ni^{2+} ions exists in the Li layers. The thin-film sample exhibits relatively lower remnant magnetization compared to that of the powder sample, which probably indicates that the thin-film sample has relatively less Li/Ni disorder.

Figure 6 compares the charge/discharge behaviors of $LiNi_{0.5}Mn_{0.5}O_2$ thin films annealed at different temperatures. Galvanostatic charge/discharge measurements were performed in the voltage range between 2.5 and 4.5 (or 4.6) V at a constant current density of 4 $\mu A/cm^2$. As shown in Fig. 6a, the charge/discharge curves for the thin film annealed at 750°C exhibit reversible voltage plateaus at about 3.75 V, agreeing well with the charge/discharge behavior of the $LiNi_{0.5}Mn_{0.5}O_2$ composite electrode as reported.[5,6] The first charge/discharge capacities are 216 and 167 mAh/g, respectively. A similar charge/discharge behavior can be observed for the 850°C annealed thin film, as shown in Fig. 6b. However, there is a very small plateau at about 3 V for the first discharge curve, probably indicating a small amount of impurity phase existing in the 850°C annealed thin film. As the annealing temperature is further increased to 950°C, the first charge/discharge curves become highly irreversible, and the 3.75 V voltage plateaus cannot be observed. Instead, a big voltage plateau above 4 V for charge and a voltage plateau between 2.5 and 3 V for discharge can be observed for the first cycle. The following second and third charge/discharge curves deliver almost no capacity, indicating a very low electrochemical activity of the film. Combined with the XRD and Raman results, the charge/discharge behaviors indicate that only thin films annealed below 850°C exist in an almost pure layered phase. Further increasing the annealing temperature induces an impurity phase formation and deteriorates the electrochemical properties of the film.

EIS is a powerful technique to determine the electrode kinetics and to isolate contributions from different kinetic processes. For the EIS measurements, the thin film annealed at 750°C was used as its electrochemical behavior agrees well with the layered $LiNi_{0.5}Mn_{0.5}O_2$ composite electrode. EIS spectra measured at different electrode potentials from 3.0 to 4.6 V (Fig. 7a and b) show that most of the impedance spectra consist of three different regions: (*i*) one small semicircle at a high frequency region, (*ii*) one big semicircle at a high to medium frequency region, and (*iii*) a straight line with a slope of 45° at a low frequency region. The first small semicircle at the high frequency region is usually attributed to the Li-ion migration through the interface between the surface layer of the film and the electrolyte.[20,21] The second big semicircle is attributed to the charge-transfer process at the electrode–electrolyte interface. The straight line at the final stage corresponds to the solid-state diffusion of Li ions into the film. Clearly, the impedance spectra of the thin-

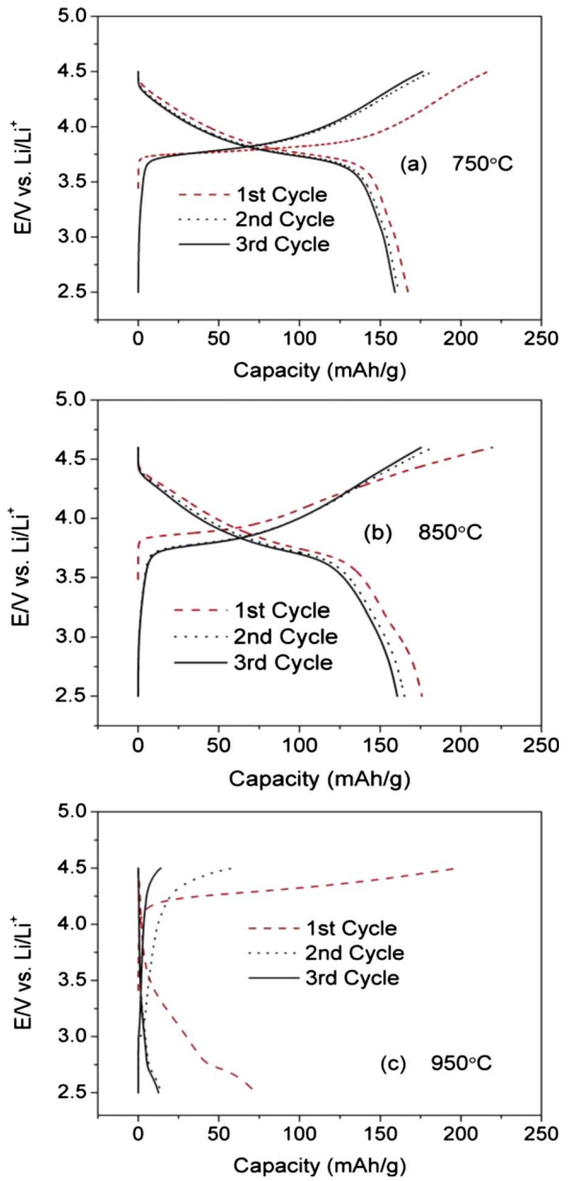

Figure 6. (Color online) First three cycles' charge/discharge curves of the $LiNi_{0.5}Mn_{0.5}O_2$ thin-film electrodes annealed at different temperatures: (a) 750, (b) 850, and (c) 950°C.

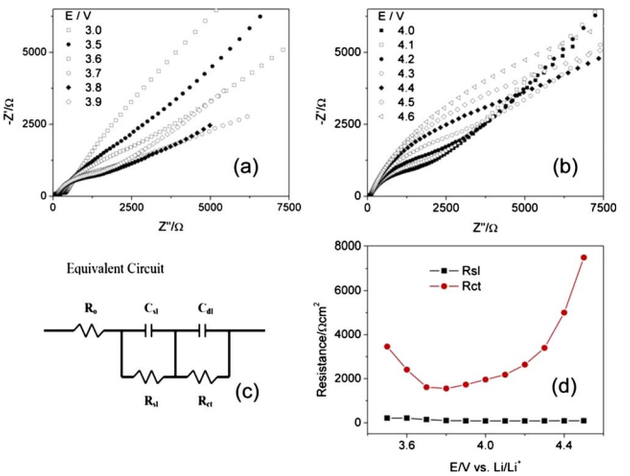

Figure 7. (Color online) [(a) and (b)] EIS spectra of the $Li/LiNi_{0.5}Mn_{0.5}O_2$ cell (750°C annealed thin-film electrode) at different charge states, (c) equivalent circuit used for fitting the experimental data, and (d) R_{ct} and R_{sl} vs electrode potential.

film electrode are highly dependent on the electrode potential. To analyze the impedance spectra, an equivalent circuit, as shown in Fig. 7c, is used to fit the experimental data. The equivalent circuit consists of a bulk electrolyte resistance (R_o), surface film resistance (R_{sl}), associated capacitance (C_{sl}), charge-transfer resistance (R_{ct}), and double-layer capacitance (C_{dl}). R_{sl} and R_{ct} at different electrode potentials obtained by fitting the experiment data with the equivalent circuit are shown in Fig. 7d. R_{ct} starts to decrease as Li is initially extracted from the $LiNi_{0.5}Mn_{0.5}O_2$ host. It reaches a minimum at about 3.75 V, then starts to increase as more Li is extracted, and increases significantly above 4.3 V. A similar behavior for the charge-transfer resistance of the composite $LiNi_{0.5}Mn_{0.5}O_2$ electrode was observed by Shaju et al.[22] in the voltage range between 3.7 and 4.3 V. A very high charge-transfer resistance of the $LiNi_{0.5}Mn_{0.5}O_2$ composite electrode at 4.6 V was also reported by Li et al.[23] and Zhang et al.[24] The initial decrease in R_{ct} is probably due to the enhancement of electronic conductivity as Li is removed from the lattice leading to the creation of mixed valent ions, Ni^{2+}/Ni^{3+} (or Ni^{4+}).[22,25] At a very high voltage, it is near the end-of-charge and the available mixed valent ions are getting reduced, leading to an inefficient electronic charge transfer.[22] For R_{sl}, the value is small and almost remains constant in the full potential range, which indicates that the surface layer contribution does not impart change in impedance with varying degree of deintercalation.

Rate capability is one of the important electrochemical properties for electrode materials, especially for those with high power applications. To study the rate capability of the present $LiNi_{0.5}Mn_{0.5}O_2$ thin-film electrode (750°C annealed sample), the cell was charged to 4.5 V at a constant current density of 2 $\mu A/cm^2$ and discharged to 2.5 V at different current densities from 2 to 50 $\mu A/cm^2$. The discharge curves of the $LiNi_{0.5}Mn_{0.5}O_2$ thin-film electrode at different current densities are shown in Fig. 8. It can be seen that the discharge capacity is highly dependent on the current density. As the current density increases, the discharge potential curve keeps lowering with an increase in cell polarization, leading to a decrease in the available capacity. The discharge capacity decreases from 175 to 112 mAh/g as current density increases from 2 to 50 $\mu A/cm^2$. As we assume the discharge capacity at 2 $\mu A/cm^2$ as the full capacity, about 65% of its full capacity can be maintained at a high current density of 50 $\mu A/cm^2$. This rate capability is poor compared to those of the $LiCoO_2$ and $LiNi_{0.5}Mn_{1.5}O_4$ thin-film electrodes in our

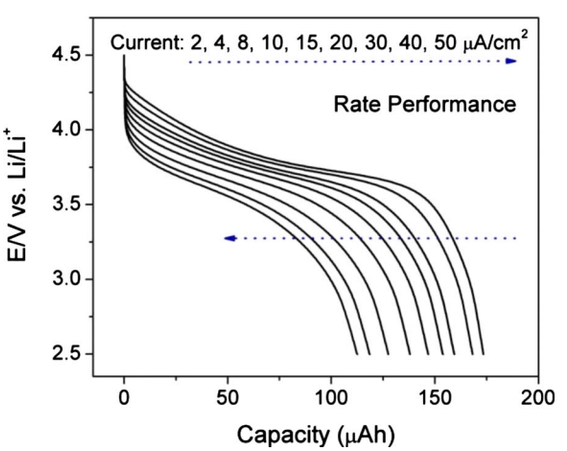

Figure 8. (Color online) Discharge curves of the $LiNi_{0.5}Mn_{0.5}O_2$ thin-film electrode (750°C annealed sample) at different current densities.

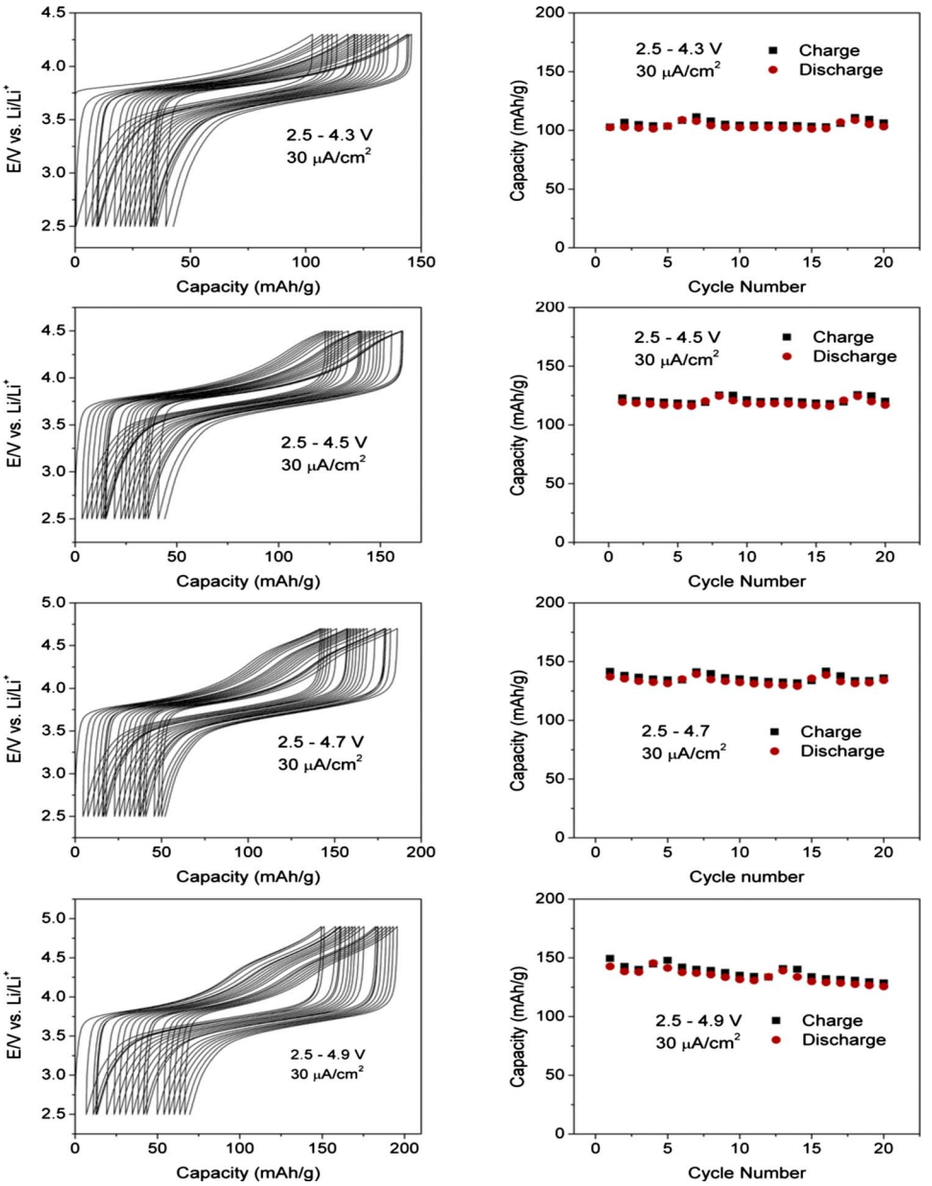

Figure 9. (Color online) Charge/discharge curves and capacity vs cycle number for different voltage windows for the $LiNi_{0.5}Mn_{0.5}O_2$ thin-film electrode (750°C annealed sample).

previous works (all thin-film samples have similar loadings and thicknesses).[3,26] For example, the 500 nm thick spinel $LiNi_{0.5}Mn_{1.5}O_4$ thin-film electrode can maintain 94% of its full capacity at a current density of 100 $\mu A/cm^2$.[3] We attribute the poor rate capacity of the $LiNi_{0.5}Mn_{0.5}O_2$ thin-film electrode to a certain amount of Li/Ni disorder in the structure as proved by the magnetization curve measurements. As discussed by Kang et al.,[4] the introduction of Ni in the Li layers not only blocks the Li diffusion channels but also attract the neighboring TMO_2 (TM = Ni and Mn) layers, thus lowering the Li mobility. Therefore, the rate capability of the $LiNi_{0.5}Mn_{0.5}O_2$ thin-film electrode is highly dependent on the degree of the Li/Ni disorder in the structure.

One of the advantages of $LiNi_{0.5}Mn_{0.5}O_2$ over $LiCoO_2$ is its good structural stability especially at high voltage (low Li content). Due to the poor structural stability, a $LiCoO_2$ electrode often show fast capacity fade when cycled with a high upper cutoff voltage (>4.5 V). To investigate the cycle performance of the $LiNi_{0.5}Mn_{0.5}O_2$ thin-film electrode (750°C annealed sample), 20 cycle charge/discharge measurements were performed on the $Li/LiNi_{0.5}Mn_{0.5}O_2$ cell at a current density of 30 $\mu A/cm^2$ in different voltage windows, 2.5–4.3, 4.5, 4.7, and 4.9, respectively. The charge/discharge curves and capacity vs cycle number for the different voltage windows are shown in Fig. 9. It can be seen that the $LiNi_{0.5}Mn_{0.5}O_2$ thin film exhibits good cycle stability (almost no capacity fade). The cycle stability is not influenced by increasing the upper cutoff voltage from 4.3 to 4.7 V. When the upper cutoff voltage is further increased to 4.9 V, slight capacity fade can be observed. The reversible capacity increases from about 100 to 150 mAh/g as the upper cutoff voltage increases from 4.3 to 4.9 V. However, the increase in the reversible capacity is not remarkable when the upper cutoff voltage is increased from 4.7 to 4.9 V. The big charge-transfer resistance of the film at high voltage such as 4.6 V (as shown in Fig. 7) could make further removal of Li at a high voltage very difficult. Therefore, under a high current density, not much more reversible capacity can be obtained by increasing the upper cutoff voltage from 4.7 to 4.9 V. Figure 10 shows the cycle performance of the thin-film electrode between 2.5 and 4.6 V at a current density of 25 $\mu A/cm^2$ for 200 cycles. The thin-film electrode exhibits excellent cycle performance with a capacity fade of about 0.03% per cycle.

It can be seen that the high voltage cycling behavior of the $LiNi_{0.5}Mn_{0.5}O_2$ thin-film electrode is different from that of the

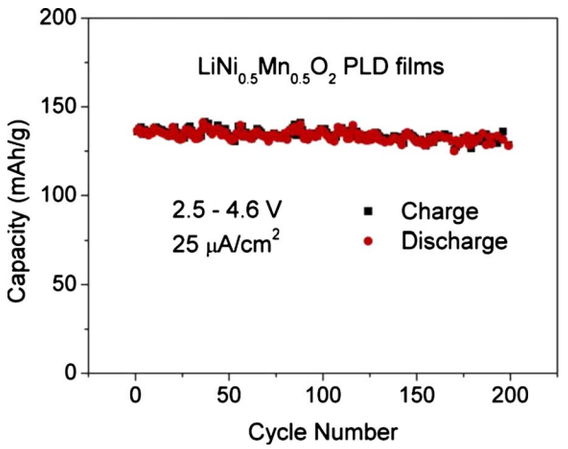

Figure 10. (Color online) Cycle performance of the $LiNi_{0.5}Mn_{0.5}O_2$ thin-film electrode (750°C annealed sample) between 2.5 and 4.6 V at a current density of 25 $\mu A/cm^2$ for 200 cycles.

$LiCoO_2$ thin-film electrode. In our previous study,[27] it has been found that the $LiCoO_2$ thin-film electrode exhibits fast capacity fade when the film is cycled above 4.5 V. The fast capacity fade at a high voltage for $LiCoO_2$ has been attributed to the two-phase transitions at high voltages. Such phase transitions may not happen in $LiNi_{0.5}Mn_{0.5}O_2$ as Ni in the Li layer can work as an anchor to stabilize the structural framework of the host.[28] The phase transitions of Li_xCoO_2 at high voltages are accompanied with severe changes in the *c*-lattice parameter. As discussed in our previous paper,[27] lattice parameter changes due to phase transitions or compositional variations are most detrimental when they occur with high Li composition gradients, which leads to a large compatibility strain in the crystallites and fast capacity fade as a consequence. Compared to the variations in the *c*-lattice parameter of Li_xCoO_2, the *c*-lattice parameter of $Li_xNi_{0.5}Mn_{0.5}O_2$ remains remarkably stable with Li concentration.[29,30] This is confirmed by an ex situ XRD measurement on the thin-film electrode at different charge states (850°C annealed thin-film samples are used as they exhibit strong XRD peaks and similar electrochemical properties to the 750°C annealed samples). The XRD spectra of the $LiNi_{0.5}Mn_{0.5}O_2$ thin-film electrode at different charge states from as-deposited to 5 V are shown in Fig. 11a. It can be seen that no obvious peak shift or peak intensity degradation occur when the film goes through different charge states. As the (003) peak is the only strong peak that can be observed from the film, the (003) peaks of XRD spectra at different charge states in a selected range of angles are shown in Fig. 11b. As shown in Fig. 11b, the (003) peak first shifts to a lower angle when charged to 4.2 V, then shifts toward a higher angle when further

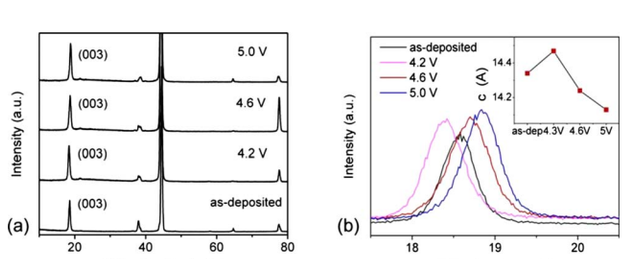

Figure 11. (Color online) (a) XRD spectra of the $LiNi_{0.5}Mn_{0.5}O_2$ thin-film electrode (850°C annealed sample) at different charge states and (b) (003) peak of the $LiNi_{0.5}Mn_{0.5}O_2$ thin-film electrode at different charge states in a selected range of diffraction angles (inset shows the *c*-lattice variation with electrode potential).

charged above 4.2 V, and keeps shifting toward higher angles with increasing charge voltage. A shift in the (003) peak with a decreasing Li content exhibits exactly the same trend as that of the $LiCoO_2$ thin-film electrode. Based on the (003) peak in Fig. 11b, the *c*-lattice parameters at different charge states are calculated to be 14.34, 14.47, 14.24, and 14.13 Å for the as-prepared film, the film charged to 4.2, 4.6, and 5.0 V, respectively (the inset in Fig. 11b). The variation in the *c*-lattice of $LiNi_{0.5}Mn_{0.5}O_2$ with Li content can be explained in a similar way as $LiCoO_2$. As Li is initially removed from $LiNi_{0.5}Mn_{0.5}O_2$, the repulsive interactions between the negatively charged oxygen planes are less compensated by the Li^+–O^{2-} interaction, resulting in an increased *c*-lattice parameter. When the Li content is reduced below $x = 0.5$ (above 4.2 V), the average charge on the oxygen ions decreases and the electrostatic repulsion between the oxygen ions is lowered, resulting in a contraction of the host along the *c*-axis. Although the variation in the *c*-lattice of the $LiNi_{0.5}Mn_{0.5}O_2$ film exhibits the same trend as that of $LiCoO_2$, the magnitude of the variation in the $LiNi_{0.5}Mn_{0.5}O_2$ film is much smaller than that of the $LiCoO_2$ thin film. As shown in Fig. 11b, the shift of the (003) peak of the $LiNi_{0.5}Mn_{0.5}O_2$ film between the as-prepared state and 5.0 V state is less than 1°, while the shift of the (003) peak of the $LiCoO_2$ thin film[27] between the as-prepared state and the 4.8 V state is nearly 2°. The (003) peak of the $LiNi_{0.5}Mn_{0.5}O_2$ film keeps its sharpness and intensity even when charged to 5 V, indicating no degradation of crystal structure. However, for a $LiCoO_2$ thin film, the (003) peak becomes broad and weak when charged to 4.8 V, indicating a severe degradation of the crystal structure. It is speculated that a certain amount of Ni ions that stays in the Li layers eventually prevents the *c*-lattice parameter of $LiNi_{0.5}Mn_{0.5}O_2$ from shrinking to an extremely small value such as that found for CoO_2.[29] The smaller variation in the *c*-lattice parameter is considered to be the reason why the $LiNi_{0.5}Mn_{0.5}O_2$ film can be reversibly cycled between 2.5 and 4.7 V without any obvious deterioration. The slight capacity fade observed when the film is cycled between 2.5 and 4.9 V may not be attributed to the structure change but to the electrolyte decomposition at such a high voltage accelerating the formation of the surface layer, which keeps increasing the cell impedance.

Conclusions

Postannealing temperature plays an important role in controlling the structure and morphology of $LiNi_{0.5}Mn_{0.5}O_2$ thin films prepared by PLD. Although a high degree of crystallinity of the film can be achieved at a high annealing temperature of 950°C, impurity phases form due to the Li loss during the heating process. XPS measurements indicate that most Ni and Mn in the film annealed at 750°C exist in the 2+ and 4+ oxidation states, respectively. Magnetic property measurements indicate the existence of a certain amount of Li/Ni disorder in the layered $LiNi_{0.5}Mn_{0.5}O_2$ thin film, which agrees well with the report on the $LiNi_{0.5}Mn_{0.5}O_2$ powders. Charge/discharge behaviors further confirm the layered structure of the $LiNi_{0.5}Mn_{0.5}O_2$ thin films annealed at lower temperatures (750 and 850°C). EIS measurements exhibit high charge-transfer resistance at a high voltage, indicating a low electrochemical activity of the film at a very high voltage. The $LiNi_{0.5}Mn_{0.5}O_2$ thin-film electrodes exhibit poor rate capability but excellent cycle performance even when cycled to a high voltage, which can be attributed to the existence of Ni in the Li layer, leading not only to sluggish Li diffusion but also to good structural stability.

Acknowledgments

This research was supported by the National University of Singapore, Agency for Science, Technology and Research through the research grant R-265-000-292-305.

National University of Singapore assisted in meeting the publication costs of this article.

References

1. R. Baskaran, N. Kuwata, O. Kamishima, J. Kawamura, and S. Selvasekarapandian, *Solid State Ionics*, **180**, 636 (2009).
2. T. Matsumura, N. Imanishi, A. Hirano, N. Sonoyama, and Y. Takeda, *Solid State Ionics*, **179**, 2011 (2008).
3. H. Xia, Y. S. Meng, L. Lu, and G. Ceder, *J. Electrochem. Soc.*, **154**, A737 (2007).
4. K. Kang, Y. S. Meng, J. Breger, C. P. Grey, and G. Ceder, *Science*, **311**, 977 (2006).
5. Z. H. Lu, L. Y. Beaulieu, R. A. Donaberger, C. L. Thomas, and J. R. Dahn, *J. Electrochem. Soc.*, **149**, A778 (2002).
6. H. Xia, S. B. Tang, and L. Lu, *J. Alloys Compd.*, **449**, 296 (2008).
7. K. Sakamoto, H. Konishi, N. Sonoyama, A. Yamada, K. Tamura, J. Mizuki, and R. Kanno, *J. Power Sources*, **174**, 678 (2007).
8. S. J. Lai, C. Hu, Y. X. Li, D. B. Luo, M. H. Cao, Z. Y. Yu, and H. X. Liu, *Solid State Ionics*, **179**, 1754 (2008).
9. H. Xia, L. Lu, and Y. S. Meng, *Appl. Phys. Lett.*, **92**, 011912 (2008).
10. T. Ohzuku and Y. Makimura, *Chem. Lett.*, **8**, 744 (2001).
11. C. Julien, *Solid State Ionics*, **136–137**, 887 (2000).
12. N. K. Karan, J. J. Saavedra-Arias, D. K. Pradhan, R. Melgarejo, A. Kumar, R. Thomas, and R. S. Katiyar, *Electrochem. Solid-State Lett.*, **11**, A135 (2008).
13. C. V. Ramana, K. Zaghib, and C. Julien, *Chem. Mater.*, **18**, 1397 (2006).
14. S. K. Martha, E. Markevich, V. Burgel, G. Salitra, E. Zinigrad, B. Markovsky, H. Sclar, Z. Pramovich, O. Heik, D. Aurbach, et al., *J. Power Sources*, **189**, 288 (2009).
15. C. M. Julien, F. Gendron, A. Amdouni, and M. Massot, *Mater. Sci. Eng., B*, **130**, 41 (2006).
16. C. Julien, M. A. Camacho-Lopez, L. Escobar-Alarcon, and E. Haro-Poniatowski, *Mater. Chem. Phys.*, **68**, 210 (2001).
17. H. Xia, L. Lu, and G. Ceder, *J. Alloys Compd.*, **417**, 304 (2006).
18. K. M. Shaju, G. V. Subba Rao, and B. V. R. Chowdari, *Electrochim. Acta*, **48**, 1505 (2003).
19. J. Xiao, N. A. Chernova, and M. S. Whittingham, *Chem. Mater.*, **20**, 7454 (2008).
20. D. Aurbach, M. Levi, E. Levi, H. Teller, B. Markovsky, G. Salitra, and U. Heider, *J. Electrochem. Soc.*, **145**, 3024 (1998).
21. M. Levi, G. Salitra, B. Markovsky, H. Teller, D. Aurbach, and L. Heider, *J. Electrochem. Soc.*, **146**, 1279 (1999).
22. K. M. Shaju, G. V. Subba Rao, and B. V. R. Chowdari, *Electrochim. Acta*, **49**, 1565 (2004).
23. D. C. Li, Y. Sasaki, K. Kobayakawa, and Y. C. Sato, *J. Power Sources*, **157**, 488 (2006).
24. B. Zhang, G. Chen, P. Xu, and C. C. Li, *J. Power Sources*, **176**, 325 (2008).
25. M. V. Reddy, G. V. Subba Rao, and B. V. R. Chowdari, *J. Phys. Chem. C*, **111**, 11712 (2007).
26. H. Xia and L. Lu, *Electrochim. Acta*, **52**, 7014 (2007).
27. H. Xia, L. Lu, Y. S. Meng, and G. Ceder, *J. Electrochem. Soc.*, **154**, A337 (2007).
28. A. Van der Ven and G. Ceder, *Electrochem. Commun.*, **6**, 1045 (2004).
29. G. G. Amatucci, J. M. Tarascon, and L. C. Klein, *J. Electrochem. Soc.*, **143**, 1114 (1996).
30. Z. H. Lu and J. R. Dahn, *J. Electrochem. Soc.*, **149**, A815 (2002).